Design and Fabrication of Line-Defect Waveguides in Hexagon-Type SOI Photonic Crystal Slabs

Cazimir G. Bostan*[a], René M. de Ridder[a], Vishwas J. Gadgil[a], Henry Kelderman[a], Laurens Kuipers[a,b], Alfred Driessen[a]
[a]University of Twente, MESA+ Research Institute, P.O. Box 217, 7500 AE Enschede, The Netherlands;
[b]FOM–Institute for Atomic and Molecular Physics (AMOLF), Kruislaan 407, 1098 SJ Amsterdam, The Netherlands.

ABSTRACT

We present a novel design approach for line-defect waveguides integrated in a photonic crystal slab (PCS) with hexagonal holes in a triangular lattice (aka 'hexagon-type'). Triangular air inclusions are symmetrically added on each side of the waveguide. Size and position of these inclusions are tuning parameters for the band diagram and can be used for minimizing the distributed Bragg reflection (DBR) effect. The waveguides show single-mode behavior with reasonably high group velocity and large transmission window, inside the gap between even-like modes. Qualitative design rules were obtained from 2D calculations based on effective index approximation and full 3D calculations of the band structure were applied for fine-tuning of structural parameters of these high-index contrast systems. Transmission spectra and losses of finite-sized structures were estimated by means of 3D finite-difference time domain (FDTD) calculations. We present a pattern definition technique, which is an integration of optical lithography with focused ion beam (FIB) high-resolution etching. The mask pattern is transferred into the SOI stack by a subsequent reactive ion etching (RIE) process. The combination of moderate resolution optical lithography and FIB etching provides an excellent tool for fast prototyping of PCS-based devices.

Keywords: photonic crystal, line defect waveguide, effective index, finite difference time domain, focused ion beam

1. INTRODUCTION

In a previous paper[1] we showed that gaps in *guided* modes (i.e. below the light-cone) may exist in a hexagon-type photonic crystal slab, even in the case of vertical asymmetry (e.g. SOI system). However, these gaps manifest themselves only below the light cone (the lowest dispersion curve of the claddings). As soon as the dispersion curves of guided modes reach the light cone boundary and become guided resonances[2], they cross the gap; then mode coupling between guided and leaky modes is likely and this leads to propagation losses. The absence of guided modes in a frequency region has potential applications in light extraction enhancement from a point-like cavity, through increasing the in-plane quality factor. The gaps in guided modes obtained for high air filling factors are situated at higher frequencies. This has a number of practical disadvantages when linear defects are introduced: (i) The higher frequencies in the band diagram are more sensitive to small variations in geometry parameters (due to e.g. fabrication imperfections); (ii) Propagation losses are roughly proportional with the area of air holes[3].
Theoretical and experimental studies have almost exclusively concentrated on a triangular lattice of circular holes. The 'defect-free' air bridge slab has a large robust gap in even modes between the first two bands. Odd modes did not receive much attention. In practice is very difficult to achieve *perfect* vertical symmetry and mode coupling due to symmetry breaking is critical[4].
Hexagonal holes provide the same large gap as their circular counterpart and also add some flexibility in design of line defects. An extra degree of freedom is the rotation angle of the hexagons with respect to their symmetry axis, this can be used to tune the waveguide shape and width. In this paper we present a study of linear defect waveguides in hexagon-type SOI slabs and a way of tuning 'defect' modes by means of triangular air inclusions (see e.g. Figure 4). These inclusions can be used to tune the waveguide width (i.e. modify the effective index of the waveguide) independently of the lattice constant and in some cases *without* lattice distortion and also minimize the effect of boundary corrugations.

* e-mail: c.g.bostan@el.utwente.nl ; phone: +31-53-4892665

The result is a waveguide (bandgap-guided in the slab plane) that resembles a ridge waveguide, showing single-mode behavior below the light cone, with high group velocity and relatively large transmission window.

2. DESIGN AND SIMULATION

2.1. Propagation phenomena in line defect waveguides

Usual waveguides made by omitting a row of holes in an otherwise periodic slab (so called W1 waveguides) have several guided modes in the gap, so that there is no truly single-mode range available[5]. These modes are pulled down from the 'air' band and they are flat at the Brillouin zone edge. Thus, they span a narrow frequency range and have a low group velocity, features that are not desirable in applications that require efficient transmission of light signals in telecom applications.

In a W1 waveguide along Γ-K direction, the lateral walls of the dielectric channel are corrugated by the neighboring rows of air holes. The corrugation is a periodic modulation of the refractive index along the waveguide axis, with periodicity a, and associated reduced Brillouin zone $(0, \pi/a)$. Therefore, a W1 waveguide looks like a 1D photonic crystal. The mechanism of gap opening and band flattening (i.e. zero group velocity) at $k = \pi/a$ can be explained in terms of destructive interference between the forward propagating waves and the waves that are contra-directionally Bragg coupled by the corrugation[6]. Partial back-reflections from individual corrugations interfere constructively, gradually converting the forward propagating wave into a backward propagating one. The energy cannot flow along the waveguide, phenomenon known as *mode gaps* or *ministop bands*. This also explains the low group velocity, especially at the edge of the line-defect Brillouin zone (which is below the light cone!).

A W1 waveguide is symmetric with respect to its middle axis, and the guided modes can be classified as odd and even with respect to it. The corrugation being symmetrical, it can couple only the same order modes with the same parity propagating in both directions along the waveguide. Dispersion curves of the modes with opposite parity can cross, regardless of mode order, while the ones of modes of same parity and different order repel each other, producing anticrossings. These anticrossings give rise to mode gaps[6].

2.2. Tuning the band diagram

Several ways of tuning the band diagram in order to obtain single-mode low-loss propagation have been proposed: (1) reducing the waveguide width by displacing blocks of holes with respect to the original lattice[7]; (2) reducing the hole-size and shifting with half-period the holes along the waveguide axis[8]; (3) increasing the hole-size[9] and changing the hole-shape into elliptical[10] along the waveguide axis; (4) increasing the hole-size for the two rows adjacent to the W1 waveguide[5]; (5) changing the corrugation symmetry either by offsetting two blocks of a perfect lattice[5, 11], gliding two separate PhC blocks or omitting an even number of lines; (6) reducing the refractive index of a W1 waveguide[9] (e.g. by etching pores into it); (7) inserting air trenches on each side of a W1 waveguide[12].

Changing the waveguide width destroys the periodicity of the original lattice and makes it more difficult to introduce bends and junctions. Approaches (1) and (5) are not convenient from this point of view. Increasing the hole-size can lead to higher losses if the mode profile has a significant overlap with the holes.

Only approaches (5) and (7), have solved the DBR problem in line defect waveguides. Lau and Fan[12] applied structural tuning without lattice distortion. The structure is a normal ridge waveguide embedded in a photonic crystal with trenches that cut through the adjacent rows of holes. The trench width is a design parameter which helps eliminating the surface states from the region of interest). The DBR effect is eliminated in this case, but this structure would have in practice a low mechanical stability and rigidity without a solid bottom cladding.

Adibi and co-workers[13] have shown that the most important role in the behavior of a line defect waveguide is played by the adjacent rows of PhC boundaries that modulate the waveguide width. In the case of circular holes, the waveguide edges will always be curved, whereas in the case of hexagonal holes, the edges can be straight. Hexagonal holes, in combination with triangular air inclusions can make linear defect waveguides that resemble a ridge waveguides.

2.3. Two-dimensional calculations based on effective index approximation

We consider 2D systems with the background dielectric medium having the effective refractive index of the fundamental guided mode of the slab system. In high-index contrast systems (like SOI) effective index approximation is valid for a narrow frequency range[14] in which the guided mode dispersion is small enough.

To avoid complications due to possible coupling to higher order modes, we choose a slab system that supports only a single mode, for both polarizations[a].
We discuss now the choice of the slab system. The most common implementation of high-index contrast PhC slabs is the 'air-bridge'[15]. This has a very good field confinement, vertical symmetry (in theory, in practice, however, is very difficult to achieve) and largest transmission window. However, the fabrication technology is quite involved and large area slabs may have a low mechanical stability. A different configuration consists in a silicon PhC slab on solid silicon dioxide cladding[7,11]. Even though mechanical stability is much improved and fabrication technology is simplified, this structure has a high degree of asymmetry and a lower transmission window. Moreover, higher losses due to radiation towards the substrate are to be expected; a thick SiO_2 buffer layer is required for bringing the losses down to an acceptable level. A compromise solution, combining the advantages of the two variants discussed above is to use a quasi-2D SiO_2 slab as a bottom cladding (i.e. the air holes penetrating both Si and SiO_2 layers of a SOI wafer). This is our present choice (see Figure 1). Etching the air holes into the bottom cladding has beneficial effects: it decreases the asymmetry and increases the frequency range below the light cone, available for truly guided modes. Moreover, the etch depth can be moderate, due to high-index contrast.

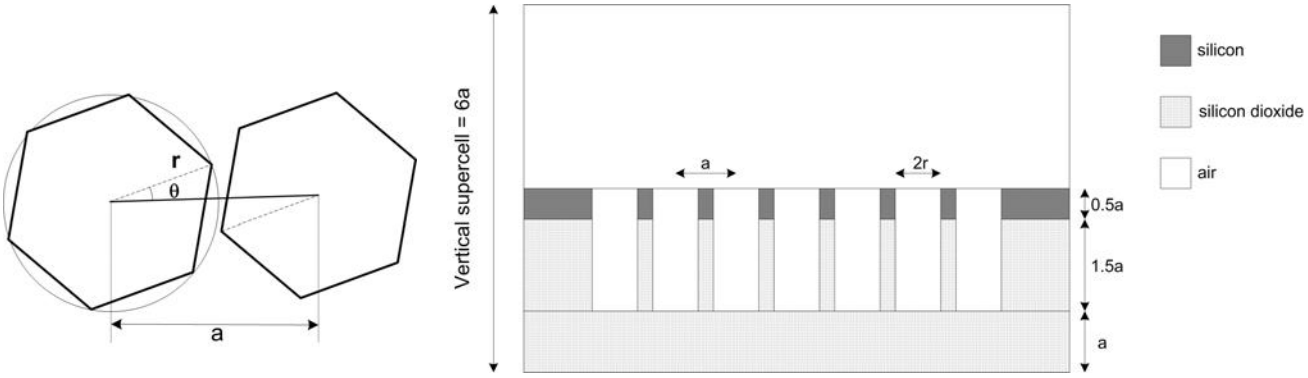

Figure 1 Geometry of SOI slab considered: top view of rotated hexagonal holes showing their geometrical parameters radius (r) and rotation angle θ (left); cross-section view of hexagonal holes penetrating the slab (right); dimensions in terms of lattice parameter *'a'* are indicated

For an asymmetric slab system consisting in a core with refractive index n and height h , sandwiched between two claddings with refractive indices n_1 and n_2 ($n_1<n_2$), the single-mode condition for free space wavelength λ_0 is[16]:

$$h_{\max} = \frac{\lambda_0}{2\pi} \cdot \frac{1}{\sqrt{n^2 - n_2^2}} \cdot \left[\pi + \tan^{-1}\left(\sqrt{\frac{n_2^2 - n_1^2}{n^2 - n_2^2}} \right) \right] \qquad (1)$$

Our design parameters are: λ_0=1.55μm, n=3.45 (Si), n_1=1 (air) and n_2=1.45 (SiO_2). Then the maximum thickness for single-mode, according to equation (1) is h_{max}=273nm. We choose a core thickness h=260nm. The effective indices of H and E guided modes will be: $n_{eff}^H = 2.924$ and $n_{eff}^E = 2.24$.

2.3.1. Band diagrams of perfect periodic lattices

We performed calculations using a numerical method based on minimization of the Rayleigh quotient in a plane wave basis using the freely available MIT Photonic Bands package[17]. There is no 2D gap in E modes for $n_{eff}^E = 2.24$. Therefore, we study only the gap maps for H modes as a function of two parameters: hexagon radius and orientation angle (see Figure 2).

[a] The convention adopted in this paper for mode classification: in 2D, modes which have the E(H) field oriented along the infinite axis are called 'E-modes' and 'H-modes', respectively; in a 3D symmetric slab, modes either even or odd with respect to the mid-plane are called 'H-like' or 'E-like'; in a 3D slab with weak asymmetry modes are classified as 'quasi H-like' or 'quasi E-like'

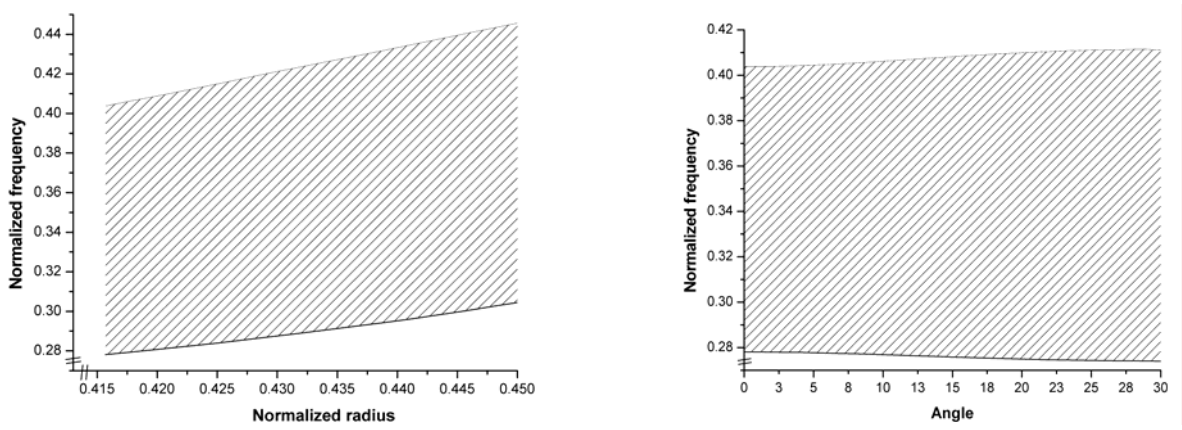

Figure 2 Gap maps as function of two parameters: radius (θ=0°)-left and angle (r=0.41a)-right

When the hole-radius is increased the gap-size increases slightly and the gap is shifted to higher frequencies.
The largest H gap is obtained for θ=30°. However, for this value of rotation angle, there is no gap for E modes (as shown before[1] the largest overlap of E and H gaps occurs for θ=9°). It is worth noting that the large H gap is maintained for the full range of rotation angles.

Introducing the air filling factor $f = 3\left(r/a\right)^2$, the effective cladding index is approximated by taking the weighted average of air and SiO_2 dielectric functions:

$$n_{eff}^{clad} = \sqrt{n_{SiO_2}^2 \cdot \left(1-f\right) + n_{air}^2 \cdot f} \tag{2}$$

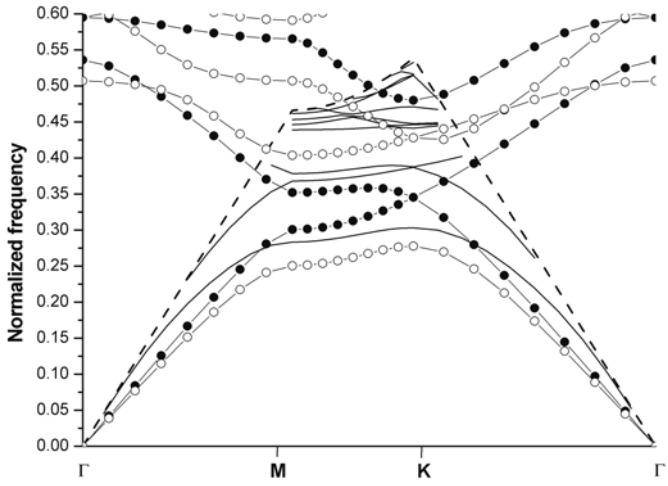

Figure 3 Comparison between the 2D bands calculated using effective index (see text for details) and 3D bands of the PhC slab shown in Figure 1 : ○ = H modes, ●=E modes, continuous line=3D bands, dashed line=light cone with effective index $n_{eff}^{clad} = 1.238$

The band structure of the PhC slab given in Figure 1, for r=0.41a and θ=0º has been calculated in 2D using this effective index approximation. The results are shown in Figure 3, where the results from a full 3D calculation are included for comparison.
Although bands are shifted upwards in frequency in 3D case, the shape of the lowest order bands is roughly preserved, allowing conclusions regarding the quasi-symmetry of modes in 3D. The effective index approximation can be efficiently applied for qualitative design of 3D photonic crystal structures (slabs and line defect waveguides).

2.3.2. Projected band diagrams and spectral transmittance of line defect waveguides

We consider line defect waveguides along Γ-K direction. Therefore the band diagram of the original perfect periodic lattice has to be projected along Γ-K. This reveals the projected gap opened between continua of states that extend in the bulk photonic crystal. When a line defect is introduced, isolated dispersion curves corresponding to states localized in the defect, appear in the projected gap. Qualitative design rules can be obtained from a 2D calculation[18] combined with the light-line of a cladding that restricts the ω-k range available for guided modes in the actual 3D case.

In order to calculate the projected band diagrams of line defect waveguides, we used a supercell (see e.g. Figure 4) containing 8 rows of holes and the line defect in the middle with the length of a (the periodicity along Γ-K). Bloch boundary conditions are applied on the sides of the supercell.

In actual experiments one is using finite-sized samples. Their behavior cannot be readily expressed in terms of Bloch modes and an important role is played by evanescent modes and reflections from the boundaries. Therefore, in order to crosscheck with the results obtained using the supercell approach, we performed a 2D finite-element (FEM) simulation using FEMLAB[19]. FEM has the advantage of outputting the stationary field profiles, so that one can quantify the field energy localization and power flow directionality. Because it is a frequency-domain method, FEM can deal with dispersion easily.

The computational domain is finite, with transparent ('low reflecting') boundary conditions. At the waveguide input a constant amplitude field is applied. Power outflow is monitored at the other end of the waveguide. Transmittance is given by the ratio between the power outflow at the output boundary and power inflow at the input boundary (it is influenced by the coupling of the input field with the waveguide modes). Frequency is scanned in the gap range $u = a/\lambda = 0.23...0.42$ with 200 steps.

In principle, angle θ can be used for designing a waveguide that does not have a central axis of symmetry. But, when the symmetry is preserved, the modes can be classified as 'even' or 'odd' with respect to the central axis, and these classes have theoretically zero cross-coupling. Then, the fundamental mode of an input ridge waveguide can preferentially excite the lowest order mode of the line defect waveguide.

Taking into account these considerations, we focus on waveguides with central symmetry axis, namely two waveguide types:

- **Type A:** lattice orientation θ=0°; waveguide width is reduced to 1.23a and air inclusions are equilateral triangles with side 0.9a (see Figure 4 left panel)
- **Type B:** lattice orientation θ=30°; lattice is undistorted and air inclusions are isosceles triangles with 120° apex angle and equal sides 1.1a (see Figure 6 left panel)**.**

Reducing waveguide width is necessary for type A waveguides in order to tune the band diagram significantly (otherwise, the projected band diagram would look very similar to that of a W1 waveguide).

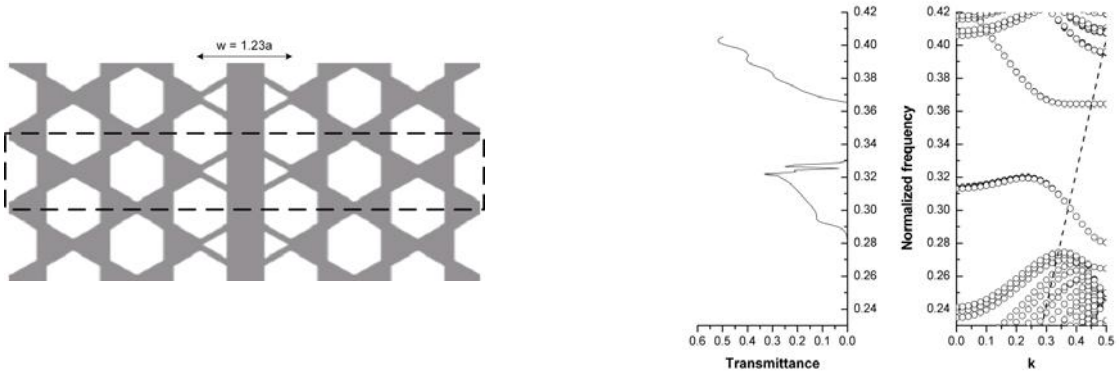

Figure 4 Type A line defect waveguide: left - domain geometry and supercell (dashed line); right - correspondence between dispersion curves of guided modes and spectral transmittance (light line is dashed)

For a type A waveguide there is a single-mode branch below the light line for u=0.28…0.3, that has a high group velocity (0.2c). There is also a large mode gap for u=0.32…0.363, and that coincides with a drastic drop in transmittance in this range (see Figure 4 right panel). This mode gap might be used for filtering, but it is a disadvantage in applications that require broadband transmission. Figure 5 shows Poynting vector amplitude plots of two modes. Both modes are localized in the 'defect', but the mode at u=0.295 has a greater expansion into the neighboring holes, and this

can increase its losses in 3D. Although situated above the light line, the mode at u=0.383 has a better localization in the high-index 'defect' and this might imply low propagation losses in practice.

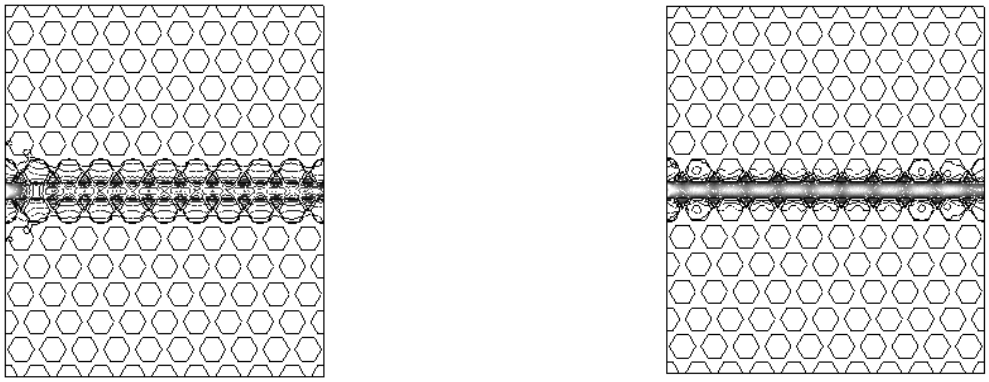

Figure 5 Contour plots of the Poynting vector amplitude for two H modes in type A waveguides at normalized frequencies u=0.295 (left) and u=0.383 (right)

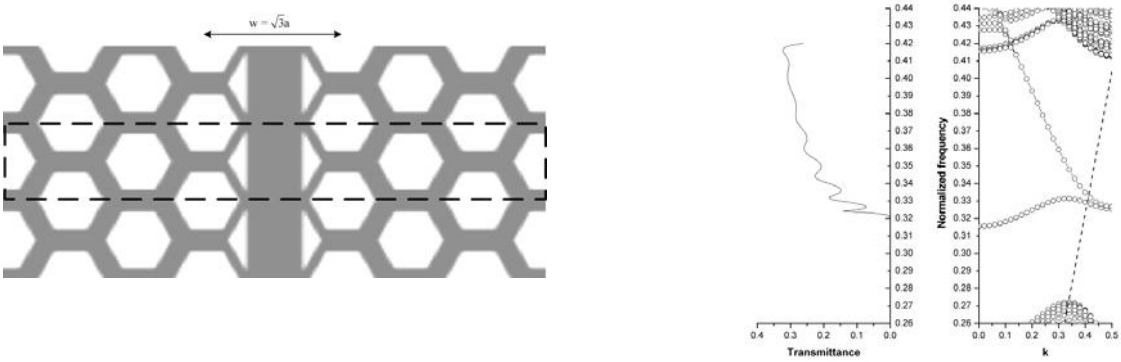

Figure 6 Type B line defect waveguide: left - domain geometry and supercell (dashed line); right - correspondence between dispersion curves of guided modes and spectral transmittance (light line is dashed)

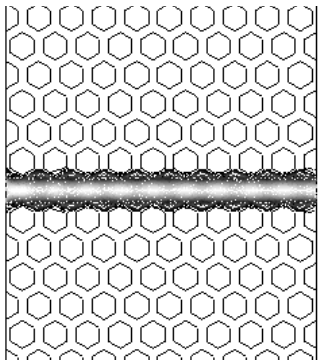

Figure 7 Contour plot of the Poynting vector amplitude for a H mode in type B waveguide at normalized frequency u=0.325

For type B waveguide there is a single guided mode whose dispersion curve is folded back at the edge of Brillouin zone with virtually no gap (this means that the DBR effect has been reduced very much). We have checked the field profiles at different frequencies and they are almost identical (one example is shown in Figure 7), supporting the single mode hypothesis. The spectral region below the light line is quite small (u=0.325…0.33) and the group velocity is smaller

than that of type A (0.05*c*) (see Figure 6 right panel). However, the broad range covered by this mode and the field localization (see Figure 7) bear promise for practical applications (even for modes situated above the light line the propagation losses might be low).

2.4. Three-dimensional finite-difference-time-domain (FDTD) calculations

High-index contrast systems require full 3D calculations of the band structure and further optimization of structural parameters. Therefore, we have analyzed by 3D FDTD a type B waveguide (see Figure 1 right panel for a cross-section view). Lattice constant is a=0.325λ_0, where λ_0=1.55μm is the central wavelength of the spectrum of interest. The normalized frequency u=0.325 is below the bulk states for the quasi E-like modes and in the gap of quasi H-like modes (see Figure 3).

The waveguide length is 14a and discretisation is 16 points/a. 'Perfectly matched layers' that approximate well the transparent boundary conditions surround the computational domain. The input wave is a Gaussian pulse with central wavelength λ_0 and width 0.5λ_0. The source is located at the center point of Si line waveguide and has a Gaussian spatial distribution resembling the fundamental mode of the ridge. The input power is normalized to unity. Power flow is monitored at the waveguide output (integrated over a detector area which cross-sections the waveguide core only). Through a 'fast Fourier transform' of the temporal response, the spectral transmittance of the waveguide (shown in Figure 8), normalized with respect to the input spectrum, is obtained at the end of a single run.

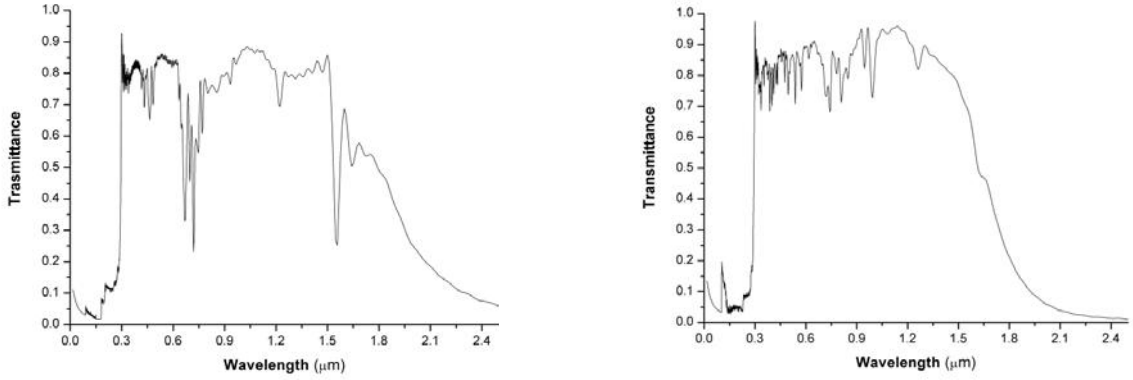

Figure 8 Transmittance of a type B waveguide calculated by 3D FDTD; left: H-like excitation (TE); right: E-like excitation (TM)

We have considered both H-like and E-like excitations, to account for the possible mode mixing. Both polarizations show quite large bandwidth of high transmittance. However, it is still unclear which factor, mode mismatch or out-of-plane losses has more weight in these results. In order to quantify the losses for λ_0, we performed another series of calculations using a continuous wave excitation. After reaching the steady state, the optical power was evaluated at several cross-sections of the waveguide, allowing to make a distinction between coupling loss and propagation loss. It turned out that, for the present set of parameters, the losses are about 15dB/mm for H-like excitation and 200dB/mm for E-like excitation. The high losses in the E-like excitation case are due to coupling to the bulk states for this polarization.

3. FABRICATION•

Several fabrication techniques for photonic crystal devices have been proposed. Deep UV laser lithography[20] is parallel, fast and expensive (requires steppers). However, it cannot reproduce sharp corners (because of optical diffraction) and proximity effects need to be compensated at the mask design level. Laser interference lithography (LIL)[21] is fast, cheap and suitable for large area PCS. On the downside, it is difficult to introduce defects precisely aligned with other integrated optical components (e.g. ridge waveguides used for light in/out coupling). E-beam lithography[22] is the most popular method for fabricating PCS. It is very precise (typical resolution 5 nm) but it is serial, hence slow, and needs proximity correction. For large design areas, stitching errors may become noticeable. Usually it is necessary to transfer

• The fabrication results presented in this section were obtained before the developments in the design; although we refer here to a different geometry, the results prove the potential of the fabrication technique

the pattern from resist to another material, more resistant to reactive ion etching (RIE). Focused ion beam (FIB) has been applied for bulk micromachining of macroporous silicon in order to fabricate 3D Yablonovite-like photonic crystals[23]. Here we apply FIB for planar definition of patterns. FIB has a resolution close to E-beam, and does not need proximity correction if used on conducting surfaces. Moreover, it provides direct transfer of the pattern into an etch resistant mask (metal) and can be integrated with conventional optical lithography.

Practical photonic crystal-based photonic integrated circuits would contain both broad and fine features: waveguides (few millimeters long and microns wide) and fiber coupling sections on the one hand and photonic crystal arrays (with lattice constants around 500 nm) on the other hand.

Writing the broad features using E-beam is expensive and time-consuming, especially from the replication point of view. Broad features can be easily and fast transferred to the wafer level by using optical lithography. Photonic crystals for optical frequencies require nm resolution, which can be obtained with FIB. In our view, the combination of moderate resolution optical lithography and FIB etching provides an excellent tool for fast prototyping of PCS-based devices.

The fabrication process goes as follows:

a) sputtering of a thin chromium layer (70nm) on the SOI wafer;
b) optical lithography for defining the in/out ridge waveguides and the PCS area between them;
c) pattern transfer into the chromium layer by wet chemical etching;
d) FIB etching of sub-micron holes; the array of holes is aligned with the coarse metal pattern by using FIB imaging
e) reactive ion etching (RIE) of the Si and SiO_2 layers using a two-step process
f) removing the chromium mask
g) cross-section analysis

The FIB system is a FEI FIB 200 single beam workstation with Ga^+ liquid metal ion source. The ion acceleration energy is 30 keV. A beam current of 70pA has been used for milling pixel-by-pixel at a resolution 4096x4096.

Our approach uses FIB as a 'lithographic' tool. This means that we are etching shallow holes, and the common problem of tapered sidewalls that occurs when the aspect ratio is close to unity is eliminated here. Another phenomenon that takes place in FIB etching is implantation of Ga^+ ions into the substrate. In our process, the 'contaminated' layer is removed in the subsequent RIE process.

Figure 9 shows a structure where a conventional mask with about 1 μm resolution defines the dielectric waveguides and areas where PhC's will be defined in a metal layer. The figure shows that FIB resolution is suitable for defining non-circular holes.

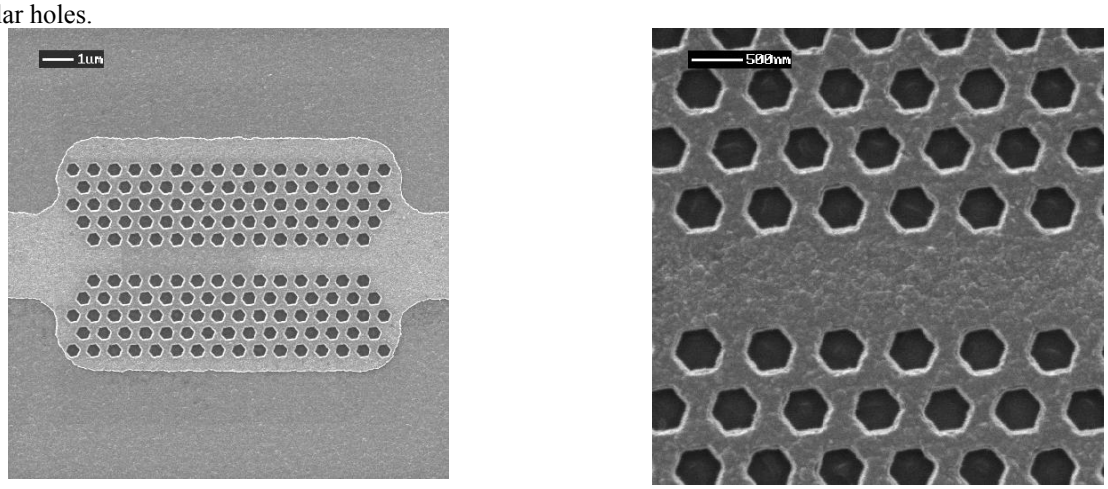

Figure 9 Left: FIB-etched hexagon-type photonic crystal pattern, aligned with waveguide pattern defined by conventional lithography in chromium. Right: detailed view.

RIE has been performed in a Electrotech, Plasmafab 310-340 parallel-plate system with an RF generator operating at 13.56 MHz. For etching Si we applied a recipe based on $SF_6/CHF_3/O_2$ gas mixture and a pressure of 100mTorr, tuned for high anisotropy and low roughness, by using the 'black silicon method'[24]. Etching SiO_2 was performed in a CHF_3/O_2 gas mixture and 10mTorr pressure.

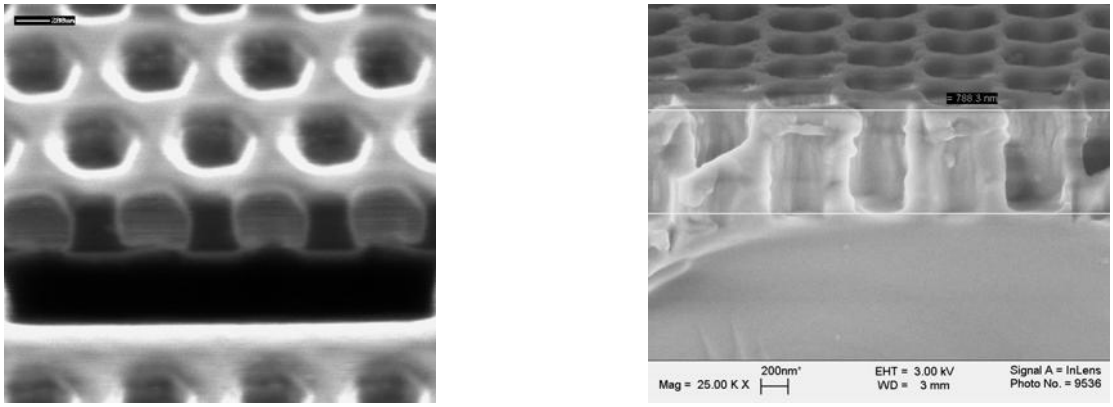

Figure 10 Left: FIB cross-section showing the profile of top Si layer after RIE; Right: SEM picture of a cleaved cross-section showing the profile of Si/SiO_2 layers after RIE

Cross-sections views of the Si and SiO_2 layers after RIE are shown in Figure 10. FIB cross-sectioning works very well for analysis of local profile analysis. Cleaving can lead to damaging of the interface (see Figure 10 right panel).

4. CONCLUSIONS

We presented a design approach for line-defect waveguides in 'hexagon-type' PCS, based on a novel way of tuning 'defect' modes by means of triangular air inclusions. The size and positions of these inclusions modify the effective index of the waveguide independently of the lattice constant (in some cases without lattice distortion) and also minimize the effect of boundary corrugations. The waveguides are integrated in a hexagon-type PCS and they have the following characteristics: reduced DBR effect, single-mode, reasonably high group velocity and large transmission window. The effective index method, allowing for efficient 2D calculations, proved to give qualitative results which could be used for a first design. The design was verified using 3D FDTD calculations which revealed low losses for H-like excitation and large transmission bandwidth of asymmetric SOI structures. We presented a pattern definition technique, which is an integration of optical lithography with FIB high-resolution etching. The combination of moderate resolution optical lithography and FIB etching provides an excellent tool for fast prototyping of PCS-based devices.

ACKNOWLEDGEMENTS

C.G. Bostan thanks H. Jansen and M. de Boer for their advice on reactive ion etching process and A.M. Otter and M. Smithers for taking some of the SEM pictures. This work was supported by the Dutch Technology Foundation STW and the MESA$^+$ SRO Advanced Photonic Structures.

REFERENCES

1. C.G. Bostan and R.M de Ridder "Design of photonic crystal slab structures with absolute gaps in guided modes", *J. Opt. Adv. Mat.*, vol. **4**, pp.921-928, 2002.
2. S.H. Fan and J. D. Joannopoulos "Analysis of guided resonances in photonic crystal slabs", *Phys. Rev.B* vol. **65**, art. no.-235112, 2002
3. R. Ferrini, R. Houdré, H. Benisty, M. Qiu and J. Moosburger "Radiation losses in planar photonic crystals:two-dimensional representation of hole depth and shape by an imaginary dielectric constant.", *J. Opt. Soc. Am.B* vol. **20**, pp.469-478, 2003
4. Y. Tanaka, T. Asano, Y. Akahane, B.S. Song and S. Noda "Theoretical investigation of a two-dimensional photonic crystal slab with truncated cone air holes", *Appl. Phys. Lett* vol. **82,** pp.1661-1663, 2003
5. M. Lončar, J. Vučković and A. Scherer "Methods for controlling positions of guided modes of photonic-crystal waveguides", *J. Opt. Soc. Am. B* vol. **18,** pp. 1362-1368, 2001
6. M. Agio and C.M. Soukoulis "Ministop bands in single-defect photonic crystal waveguides", *Phys. Rev. E* vol. **64**, art. no.-055603, 2001

7. M. Notomi, A. Shinya, K. Yamada, J. Takahashi, C. Takahashi, and I. Yokohama "Structural tuning of guiding modes of line-defect waveguides of silicon-on-insulator photonic crystal slabs", *IEEE J. Quantum. Electron*., vol. **38**, pp. 736-742, 2002.
8. K. Yamada, H. Morita, A. Shinya, and M. Notomi "Improved line-defect structures for photonic-crystal waveguides with high group velocity", *Opt. Comm.* vol. **198,** pp. 395-402, 2001
9. T. Søndergaard and A. Lavrinenko "Large-bandwidth planar photonic crystal waveguides", *Opt. Comm.* vol. **203,** pp. 263-270, 2002
10. M. M. Sigalas and E. Chow "Elliptical air hole waveguides in slab photonic crystals", *J. Appl. Phys.* vol. **93,** pp.10125-10127, 2003
11. N. Susa "The large bandwidth and large group velocity for the single guided mode in an asymmetric photonic crystal slab waveguide", *Jpn. J. Appl. Phys.* vol. **42**, pp.L724-L727, 2003
12. W. T. Lau and S. H. Fan "Creating large bandwidth line defects by embedding dielectric waveguides into photonic crystal slabs", *Appl. Phys. Lett.* vol. **81**, pp. 3915-3917, 2002
13. A.Adibi, Y. Xu, R.K. Lee, M. Lončar, A. Yariv, and A. Scherer "Role of distributed Bragg reflection in photonic-crystal optical waveguides", *Phys. Rev. B* vol. **64,** art. no.-041102, 2001
14. M. Qiu "Effective index method for heterostructure-slab-waveguide-based two-dimensional photonic crystals", *Appl. Phys. Lett.* vol. **81**, pp. 1163-1165, 2002
15. M. Lončar, T. Doll, J. Vučković and A. Scherer "Design and fabrication of silicon photonic crystal optical waveguides", *J. Lightwave Technol.* vol. **18**, pp. 1402-1411, 2000
16. A. Yariv and P. Yeh, *Optical Waves in Crystals,* pp.420, Wiley, New York, 1984
17. S.G. Johnson and J.D. Joannopoulos "Block-iterative frequency-domain methods for Maxwell's equations in a planewave basis", *Opt. Express* vol. **8**, pp.173-190, 2001.
18. T. Søndergaard, J. Arentoft, and M. Kristensen, "Theoretical analysis of finite-height semiconductor-on-insulator-based planar photonic crystal waveguides", *J. Lightwave Technol.*, vol. **20**, pp. 1619-1626, 2002.
19. FEMLAB is a trademark of Comsol AB, Sweden, http://www.femlab.com.
20. W. Bogaerts, V. Wiaux, D. Taillaert, S. Beckx, B. Luyssaert, P. Bienstman, and Roel Baets, "Fabrication of photonic crystals in silicon-on-insulator using 248-nm deep UV lithography", *IEEE J. Sel. Topics Quantum. Electron.*, vol. **8**, pp. 928-934, 2002.
21. L. Vogelaar, W. Nijdam, H.A.G.M. van Wolferen, R.M. de Ridder, F.B. Segerink, E. Flück, L. Kuipers, and N.F. van Hulst, "Large Area Photonic Crystal Slabs for Visible Light with Waveguiding Defect Structures: Fabrication with Focused Ion Beam Assisted Laser Interference Lithography", *Adv. Mat.* vol. **13**, pp. 1551-1554, 2001.
22. Y. Xu, H.-B. Sun, J.-Y. Ye, S. Matsuo, and H. Misawa, "Fabrication and direct transmission measurement of high-aspect-ratio two-dimensional silicon-based photonic crystal chips", *J. Opt. Soc. Am. B* vol. **18** , pp. 1084-1091, 2001.
23. A. Chelnokov, K. Wang, S. Rowson, P. Garoche, and J.-M. Lourtioz, "Near-infrared Yablonovite-like photonic crystals by focused-ion-beam etching of macroporous silicon", *Appl. Phys. Lett.* vol. **77**, pp. 2943–2945, 2000.
24. H. Jansen, M. de Boer, J. Burger, R. Legtenberg, and M. Elwenspoek, "The Black Silicon Method .2. The Effect of Mask Material and Loading on the Reactive Ion Etching of Deep Silicon Trenches" , *Microelectronic Eng.* vol. **27**, pp. 475-480, 1995